AIAA JOURNAL
Vol. 40, No. 9, September 2002

Pressure Gradients in the Regenerator and Overall Pulse-Tube Refrigerator Performance

P. Mayzus,* L. Fang,* X. Deng,† O. R. Fauvel,‡ and L. Bauwens§
University of Calgary, Calgary, Alberta T2N 4N1, Canada

Significant pressure drops in the regenerator are typical in pulse-tube cryocoolers, with significant impact on performance. Irreversibilities due to viscous friction obviously lower efficiency, but in the pulse tube, this is not necessarily the most crucial issue. Indeed, by virtue of having only one driven element (the compressor), the pulse tube is a rather inflexible device from a design standpoint. Pressure and velocity amplitudes and phases determine energy fluxes. Impedances ultimately determine how large these fluxes are, hence how good a refrigerator a given design will produce. Impedance values are determined by the volume distribution, the orifice resistance, and the effect of viscous friction in the regenerator. The focus is on friction, which is difficult to deal with, especially if the device includes a bypass. An asymptotically consistent analysis has been developed, in which the regenerator is represented as an arbitrary porous medium. In contrast with most models, the analysis initially assumes arbitrary large pressure gradients and, of course, arbitrarily large temporal pressure fluctuations. The model thus obtained shows that when pressure differences due to viscous friction are comparable with the amplitude of temporal variations, viscous irreversibilities are much larger than the thermal ones. The regenerator formulation is then incorporated within a small-amplitude, harmonic model of the overall device, including the bypass, if any. For simple assumptions with respect to the temperature profile along the regenerator, such as linear and exponential profiles, closed-form solutions are obtained. Finally, the results are analyzed and their relevance is discussed.

Nomenclature

A	=	net cross-sectional area
$\mathcal{A}$	=	orifice admittance
a	=	constant describing exponential temperature profile
C_1	=	first integration constant
C_2	=	second integration constant
c	=	constant defining linear temperature profile
c_p	=	specific heat at constant pressure
c_v	=	specific heat at constant volume
$\hat{\boldsymbol{e}}_x$	=	unit vector in x direction
f	=	friction factor
i	=	$\sqrt{-1}$
$J_1(X)$	=	Bessel function of order 1 of the first kind
k	=	thermal conductivity
L	=	large length scale
l	=	small length scale (mesh size)
M	=	reference Mach number
m	=	constant, $\sqrt{[\sqrt{(a^4+4\pi^2 f^2)}+a^2]}/\sqrt{2}$
n	=	constant, $\sqrt{[\sqrt{(a^4+4\pi^2 f^2)}-a^2]}/\sqrt{2}$
Pr	=	Prandtl number
p	=	pressure
p'	=	pressure field from Eq. (10)
Re	=	reference Reynolds number
$\dot{S}$	=	entropy flux
s	=	specific entropy
T	=	temperature
t	=	time
U	=	mean instantaneous longitudinal velocity in regenerator
u	=	x component of the velocity vector
$\boldsymbol{u}$	=	velocity vector
V	=	volume inside pulse tube
$\boldsymbol{v}$	=	velocity vector from Eq. (10), $\boldsymbol{u}/U$
X	=	large-scale longitudinal coordinate
x	=	small-scale longitudinal coordinate
$Y_1(X)$	=	Bessel function of order 1 of the second kind
α	=	parameter of order 1, $M^2L/(Rel)$
γ	=	ratio of specific heats, c_p/c_v
δ	=	parameter of order 1, $\rho_{\text{ref}}c_p k_m/M^2\rho_m c_m k$
ϵ	=	small parameter, l/L
μ	=	dynamic viscosity
π	=	3.1415926535...
ρ	=	density
$\boldsymbol{\tau}$	=	deviatoric stress tensor
Ω	=	impedance
ω	=	angular speed
∇	=	differential operator, either gradient or (followed by $\cdot$) divergence

Subscripts

A	=	interface between compressor space and aftercooler
AC	=	aftercooler
B	=	bypass
CP	=	compressor
F	=	freezer
H	=	interface between regenerator and aftercooler
L	=	left (hot) regenerator end
m	=	matrix
O	=	orifice
R	=	right (cold) regenerator end
ref	=	reference state
res	=	reservoir
T	=	pulse tube

Superscripts

(0)	=	leading-order term in perturbation series
(1)	=	term of order M^2 in perturbation series
*	=	complex conjugate
~	=	dimensional quantities

Received 15 January 2000; revision received 5 February 2002; accepted for publication 11 February 2002.

*Graduate Student, Department of Mechanical and Manufacturing Engineering.
†Postdoctoral Fellow, Department of Mechanical and Manufacturing Engineering.
‡Professor, Department of Mechanical and Manufacturing Engineering.
§Professor, Department of Mechanical and Manufacturing Engineering. Member AIAA.

Introduction

MOST small-scale cryorefrigerators currently operating in the 60–80-K range are of the Stirling type. It is expected, however, that orifice-type pulse-tube devices will progressively replace Stirling technology in the coming years, as their performance improves and their cost drops.[1–3] Their key advantage is simplicity, with no moving parts on the cold side. On the other hand, with only one active element, the compressor, instead of two in Stirling refrigerators, the pulse-tube is a more inflexible device. The relative magnitudes of oscillating pressure and oscillating velocity, and their phase difference, play a crucial role in determining performance. These variables are largely determined by the interaction between volume distribution and orifice resistance,[4] but they are also affected by viscous friction in the regenerator. At lower temperatures, in contrast with noncryogenic applications of regenerators, the balance between thermal losses and viscous losses shifts toward the latter because the speed of sound drops and the Mach numbers increase. Because pressure gradients affect the phase and amplitude relationships between pressures and velocities, they affect the energy fluxes, even before accounting for the losses due to viscous irreversibilities. That is the focus of this study.

When pressure gradients are neglected in the regenerator, the interplay between orifice (and, if applicable, bypass) resistance and volume distribution is readily determined by small-amplitude analysis[5] or, equivalently, phasor diagrams.[6] In the linearized model, the current study incorporates the results of an asymptotically consistent analysis of the flow and pressure gradient in the regenerator, for assumed regenerator temperature profiles. Strictly speaking, this last assumption is not asymptotically consistent; indeed, pursued to higher order, the analysis actually determines the temperatures.[7] However, it will be shown that for reasonable assumed temperature profiles, such as the widely used linear profile,[8] closed-forms solutions are readily obtained for the entire refrigerator, which, within a reasonable range, do not vary much with temperature profiles. Thus, this model yields a useful tool, which is very fast, in particular when implemented using one of the symbolic manipulation packages available commercially. It readily provides solutions within large subsets of the parameter space, identifying peaks and trends in the selected global performance variable, such as the coefficient of performance or the refrigeration.

Fully numerical approximate solutions appear promising for pulse-tube performance prediction. However, significant challenges remain if large pressure gradients are to be solved for in a fully coupled manner. Resolving acoustics[9,10] results in numerical codes either slow or coarsely resolved. High order of accuracy requires flux limiting to avoid oscillations and may be illusory because the device geometry is only given to first order. Spaces with a linear topology are easy to resolve in one-dimensional models, but bulky volumes such as cylinder spaces are inherently three dimensional and suffer from the thorny problem of turbulence. Simple but fundamentally sound approximate models are less problematic, although not necessarily less accurate.

The current paper is organized as follows. First, the regenerator model is developed, deferring a specific description of the pulse-tube device to the next section. When the discussion is kept as general as possible, pressure amplitudes are taken as arbitrary, deferring an additional assumption, that amplitudes are small, to the next section. Crucially, the regenerator model assumes that spatial and temporal pressure variations are of comparable magnitudes. The matrix is described as an arbitrary porous medium, and a distinguished limit is introduced that relates the ratio mesh size/large length scales to the Mach number. Next, the attention shifts to entire refrigerator, starting with its complete description and a discussion of its operating principle. The small-amplitude approximation is introduced in a precise manner. From volume distribution, orifice resistance, and compressor motion, appropriate boundary conditions to the regenerator problem are obtained, with or without a bypass. The resulting boundary-value problem is then solved in closed form, assuming two different temperature profiles, linear and exponential, respectively. Finally, solutions for specific configurations illustrate how powerful the approach is and yield new insight in the role of the bypass.

Regenerator Model

Methodology and Assumptions

The regenerator model that results from the analysis in this section looks deceptively simple. It consists of full one-dimensional continuity, a one-dimensional approximation to momentum in which inertia is neglected and in which viscous effects represented by a Darcy law are balanced by pressure gradients at leading order, and, finally, a time-independent temperature profile. Temperature varies only longitudinally on a length scale comparable with the regenerator length, but it is constant on scales comparable with the mesh size. Although simple, this specific combination of the three approximate conservation equations is new. As shown here, it can be derived rigorously as a proper asymptotic limit to the complete three-dimensional problem. In contrast, in the more complete one-dimensional problem typically solved numerically,[9] the energy equation allowing for heat transfer between fluid and matrix is empirical. (The empirical one-dimensional energy equation fails to conserve energy between temporal fluctuations and advected contributions. Indeed, averaging the full energy over the cross section results in a simple transverse averaging for the first, whereas the second, following the Graetz approach,[11] requires mass flow temperature averaging.[12] For nonuniform profiles, these two averages differ; for parabolic flow, results from the one-dimensional equation demonstrably are inconsistent with the two-dimensional solution.[7]) Although the results in this section may look obvious, that they can be derived rigorously is not obvious nor unimportant. The analysis itself is not trivial, and it also provides for identification of the complete set of required assumptions.

The regenerator geometry considers a duct of finite length and uniform cross section, filled with a porous medium of arbitrary topology, details of which are not known. An equivalent one-dimensional problem is derived that represents as accurately as possible the behavior of the exact problem even though the detailed topology is not known. Two scales are introduced, one characterizing the mesh, which is very small, typically in the 40-μm range, and the other the length and diameter, with typical values in the 1–10-cm range, which are comparatively large. When a conventional multiple scale technique is used, the viscous effect on pressure gradients, which has its source on the small scale, is then allocated to the large-scale problem. A specific distinguished limit provides for leading-order pressure gradients occurring over the regenerator length.

The solution assumes that 1) Mach numbers are small; 2) arbitrarily large sweeps occur; hence a regenerator length that is short compared to the acoustic wavelength; 3) arbitrary pressure fluctuations in time occur; 4) the thermal mass of the matrix is large compared with that of the cycle fluid; and 5) to the best of our knowledge, the mesh topology is statistically uniform lengthwise. These assumptions are substantially different from usual porous media flows in the literature,[13] simpler in some respects and more complex in others. Assumptions 3 and 4 will be expressed in a precise way as the analysis proceeds.

Whenever a small Mach number assumption is made, a decision concerning lengths is unavoidable: Lengths scale either with the sweep by the fluid motion, or with acoustic wavelengths. The two possible choices yield different results. It is not the case that one is more general than the other, but given a specific situation, one may be more realistic than the other. As in previous work,[7,14] the former has been selected here. It allows for large pressure oscillations, but pressure gradients due to fluid inertia are excluded. In contrast, the acoustic model[15] is limited to small pressure fluctuations, but allows for fluid inertia to play a role. In helium at ambient temperature and at 20 Hz, acoustic wavelengths are of the order of 50 m; the sweep, smaller by a factor equal to the Mach number, is more representative of typical regenerator lengths.

Conservation Equations, Scaling, and Distinguished Limits

The problem includes conservation equations and boundary conditions. For the current purposes, the stationary regime is being sought, and the problem of interest is then a periodic boundary-value problem, which does not require initial conditions. When the dimensional variable names are indicated with a tilde, the conservation

equations include mass, momentum, energy for the fluid, and energy in the matrix:

$$\frac{\partial \tilde{\rho}}{\partial \tilde{t}} + \tilde{\nabla} \cdot (\tilde{\rho}\tilde{\boldsymbol{u}}) = 0 \tag{1a}$$

$$\tilde{\rho}\frac{\partial \tilde{\boldsymbol{u}}}{\partial \tilde{t}} + \tilde{\rho}\tilde{\boldsymbol{u}} \cdot \tilde{\nabla}\,\tilde{\boldsymbol{u}} = -\tilde{\nabla}\,\tilde{p} + \tilde{\nabla} \cdot \tilde{\boldsymbol{\tau}} \tag{1b}$$

$$\frac{\partial}{\partial \tilde{t}}\left[\tilde{\rho}c_v\tilde{T} + \frac{1}{2}\tilde{\rho}(\tilde{\boldsymbol{u}} \cdot \tilde{\boldsymbol{u}})\right] + \tilde{\nabla} \cdot \left[\tilde{\rho}\tilde{\boldsymbol{u}}\left\{c_p\tilde{T} + \frac{1}{2}(\tilde{\boldsymbol{u}} \cdot \tilde{\boldsymbol{u}})\right\} - \tilde{\boldsymbol{u}}\tilde{\boldsymbol{\tau}} - k\tilde{\nabla}\,\tilde{T}\right] = 0 \tag{1c}$$

$$\rho_m c_m \frac{\partial \tilde{T}_m}{\partial \tilde{t}} = \tilde{\nabla} \cdot k_m \tilde{\nabla}\,\tilde{T}_m \tag{1d}$$

with $\tilde{T} = \tilde{T}_m$ and $k_m\tilde{\nabla}\,\tilde{T}_m = k\tilde{\nabla}\,\tilde{T}$ at the boundaries between matrix and fluid. The energy equation (1c) results from adding the mechanical energy equation, obtained by dot-multiplying momentum by $\tilde{\boldsymbol{u}}$, to the thermal energy equation.

Next, time is scaled by the period of the compressor motion, velocity, from assumption 2, by the ratio regenerator length/period, pressure by a representative value close to the mean pressure, and temperature by some representative reference. Density is scaled by its value at the reference pressure and temperature. For length, two scales are introduced: l the mesh thickness and L the regenerator length. The parameters appearing in the dimensionless equations are the reference Mach number M equal to the reference velocity divided by the speed of sound at the reference state, the reference Reynolds number Re based on the mesh size, the Prandtl number Pr, the ratio μ of the dynamic viscosity to its value at the reference state, and the ratio of specific heats γ. From assumption 3, pressure gradients are of order unity over the long length scale L. In momentum, short-range viscous forces must then be of order unity, hence the following relationship between M and l/L (a distinguished limit):

$$(M^2/Re)(L/l) = \alpha = \mathcal{O}(1) \tag{2}$$

Likewise, assumption 4 is fairly realistic, that is, the thermal diffusivity of the matrix is higher than that of the gas. More precisely, it is assumed that δ is of order unity:

$$(\rho_{\mathrm{ref}}c_p/\rho_m c_m)(k_m/k) = M^2\delta \tag{3}$$

This leaves only one remaining independent small parameter, which is used in the perturbation scheme introduced next. When l/L is replaced by its expression in M^2 and α, the conservation laws now depend only on M^2 and parameters of order unity:

$$M^2\left(\frac{\partial \rho}{\partial t} + \frac{\partial \rho u}{\partial X}\right) + \alpha Re\nabla \cdot (\rho\boldsymbol{u}) = 0 \tag{4a}$$

$$\alpha Re\rho\boldsymbol{u} \cdot \nabla\,\boldsymbol{u} = -\frac{1}{\gamma}\left(\frac{\alpha Re}{M^2}\nabla\,p + \frac{\partial p}{\partial X}\hat{\boldsymbol{e}}_x\right) + \alpha\nabla \cdot \tau + \mathcal{O}(M^2) \tag{4b}$$

$$\frac{\alpha Re}{M^2}\nabla \cdot (\rho\boldsymbol{u}T) = \frac{\alpha}{M^2}\nabla \cdot \frac{\mu}{Pr}\nabla\,T + \mathcal{O}(1) \tag{4c}$$

$$\frac{\partial T}{\partial t} = \alpha\nabla \cdot \frac{\delta}{Pr}\nabla\,T + \mathcal{O}(M^2) \tag{4d}$$

Perturbation Solution

All variables are written as perturbation series in M^2, for instance, for velocity,

$$\boldsymbol{u} = \boldsymbol{u}^{(0)} + M^2\boldsymbol{u}^{(1)} + \cdots \tag{5}$$

Replacing into Eqs. (4) and collecting leading-order terms results in $\nabla \cdot (\rho^{(0)}\boldsymbol{u}^{(0)}) = 0$ and $\nabla\,p^{(0)} = 0$; hence, $p^{(0)} = p^{(0)}(X, t)$. The energy equations become

$$\nabla \cdot \left(\rho^{(0)}T^{(0)}\boldsymbol{u}^{(0)}\right) = \frac{1}{Re}\nabla \cdot \frac{\mu}{Pr}\nabla\,T^{(0)} \tag{6a}$$

$$\frac{\partial T^{(0)}}{\partial t} = \alpha\nabla \cdot \frac{\delta}{Pr}\nabla\,T^{(0)} \tag{6b}$$

This problem for temperatures is homogeneous both in time and in the short coordinates, with homogeneous boundary conditions. It only admits the trivial solution independent of either time and the short coordinate: $T^{(0)} = T^{(0)}(X)$. Because $p^{(0)}$ is also independent of $\boldsymbol{x}$, so is density, and $\nabla \cdot \boldsymbol{u}^{(0)} = 0$.

To the next order, only mass and momentum are needed:

$$\frac{\partial \rho^{(0)}}{\partial t} + \frac{\partial}{\partial X}\left(\rho^{(0)}u^{(0)}\right) + \alpha Re\rho^{(0)}\nabla \cdot \boldsymbol{u}^{(1)} + \alpha Re\boldsymbol{u}^{(0)} \cdot \nabla\,\rho^{(1)} = 0 \tag{7a}$$

$$Re\alpha\rho^{(0)}\boldsymbol{u}^{(0)} \cdot \nabla\,\boldsymbol{u}^{(0)} = -\frac{1}{\gamma}\left(\frac{\partial p^{(0)}}{\partial X}\hat{\boldsymbol{e}}_x + \alpha Re\nabla\,p^{(1)}\right) + \alpha\mu\nabla^2\boldsymbol{u}^{(0)} \tag{7b}$$

The goal here is to obtain a one-dimensional problem that does not depend on the short-space coordinates. To that effect, the average velocity $U(X, t)$ defined by integration over the void cross section $A(x)$ is introduced:

$$AU = \int_A \boldsymbol{u}^{(0)} \cdot \hat{\boldsymbol{e}}_x\,\mathrm{d}A \tag{8}$$

When continuity equation (7a) is integrated over A, and it is taken into account that, to all orders, velocity vanishes at the matrix walls, the usual one-dimensional continuity equation is obtained:

$$\frac{\partial \rho^{(0)}}{\partial t} + \frac{\partial}{\partial X}\left(\rho^{(0)}U\right) = 0 \tag{9}$$

Next, the vector $\boldsymbol{v}$ and the pressure field p' are introduced. They depend only on the local instantaneous Reynolds number and the local mesh topology. They are defined as the solution to the following incompressible problem, in which the local instantaneous Reynolds number $ReU\rho^{(0)}/\mu$, assumed known, is taken as a parameter:

$$\nabla \cdot \boldsymbol{v} = 0 \tag{10a}$$

$$Re\left(U\rho^{(0)}\big/\mu\right)\boldsymbol{v} \cdot \nabla\,\boldsymbol{v} = -(Re/\gamma\mu)\nabla\,p' + \nabla^2\boldsymbol{v} \tag{10b}$$

with no-slip boundary conditions at the matrix wall. When the solution is made unique, with the auxiliary condition imposing a total volumetric flow equal to unity,

$$\int_A \boldsymbol{v} \cdot \hat{\boldsymbol{e}}_x\,\mathrm{d}A = A \tag{11}$$

When these equations are multiplied by U, the incompressible flow problem described by Eq. (7b) is recovered with $\boldsymbol{u} = U\boldsymbol{v}$ if pressures are related by

$$p^{(1)} + \frac{1}{\alpha Re}x\frac{\partial p^{(0)}}{\partial X} = Up' \tag{12}$$

Next, consider the pressure difference from the two locations x^- and x^+:

$$\frac{1}{\alpha Re}(x^+ - x^-)\frac{\partial p^{(0)}}{\partial X} = \left(Up' - p^{(1)}\right)\Big|_{x^-}^{x^+} \tag{13}$$

The introduction of two length scales results in indeterminacy in the allocation of the pressure gradients between short-range gradients in $p^{(1)}$ and long-range gradients in $p^{(0)}$. However, there cannot be a nonzero mean gradient over the short scale. Thus, the indeterminacy is resolved by allocating any nonzero mean to the long range:

$$\lim_{(x^+ - x^-)\to\infty}\frac{1}{x^+ - x^-}p^{(1)}\Big|_{x^-}^{x^+} = 0 \tag{14}$$

Finally, the one-dimensional momentum equation is obtained:

$$\frac{\partial p^{(0)}}{\partial X} = -fU \tag{15}$$

When a formal (nonempirical) definition is adopted for the friction factor $f(ReU\rho^{(0)}/\mu)$,

$$f = -Re\alpha \lim_{(x^+ - x^-)\to\infty} \frac{1}{x^+ - x^-} p' \Big|_{x^-}^{x^+} \tag{16}$$

This limit is obtained from the problem for $\boldsymbol{v}$ and p'. Its value depends on X and t only through the local, instantaneous Reynolds number, and it does not vary in the transverse direction because transverse fluctuations in p' are finite. The formulation allows for f to depend on the local mesh topology at X, but usually the best assumption is to take the mesh to be statistically uniform in X. For a given matrix topology, as usual, this friction factor is then obtained from steady laminar flow experiments such as by Miyabe et al.,[16] in a geometrically similar matrix. In the laminar limit, the linear friction model typical of porous media is recovered.[13] When superscripts are dropped from leading-order density and temperature and P is used for leading-order pressure, the one-dimensional problem is

$$\frac{\partial \rho}{\partial t} + \frac{\partial}{\partial X}(\rho U) = 0 \tag{17a}$$

$$\frac{\partial P}{\partial X} = -fU \tag{17b}$$

$$T = T(X) = \frac{P}{\rho} \tag{17c}$$

Higher-order perturbations would yield an equation for leading-order temperature in the usual way,[7,14,17,18] showing inter alia that a so-called dc flow (mass flow imbalance over one period) larger than $\mathcal{O}(M^2)$ is incompatible with a leading-order longitudinal temperature gradient. Thus, any nonzero enthalpy flux, hence also any thermal irreversibility, is relegated to $\mathcal{O}(M^2)$. Viscous friction, however, results in entropy sources at leading order. The total entropy carried by the fluid at some location X in the regenerator over one period, the entropy flux $\dot{S}$, can be evaluated:

$$\dot{S} = \int_0^\tau \left(\int_A \rho u s \, \mathrm{d}A \right) \mathrm{d}t \tag{18}$$

When it is taken into account that, for an ideal gas, entropy is related to pressure and temperature by $s = \log T - (\gamma - 1)/\gamma \log p$, the leading-order entropy flux is given by

$$\dot{S}(X) = -\frac{\gamma - 1}{\gamma} \int_0^\tau \rho U \log P \, \mathrm{d}t = \frac{(\gamma - 1)}{\gamma f T} \int_0^\tau P \frac{\partial P}{\partial X} \log P \, \mathrm{d}t \tag{19}$$

If the pressure gradient is nonzero, the leading-order entropy flux is nonzero.

Pulse-Tube Model

Pulse-Tube Description

The typical pulse-tube configuration is shown on Fig. 1. At the left end of Fig. 1 picture, a piston is periodically oscillating, indicated by CP (for compression space), and produces the flow in the entire device. From left to right, the various flow passages are any unavoidable compressor dead volume, the aftercooler (a heat exchanger at ambient temperature), the regenerator, the freezer, the pulse-tube proper and, finally, an orifice connected to the reservoir: a buffer volume. A bypass between regenerator, freezer, and tube is often found to improve performance.[19]

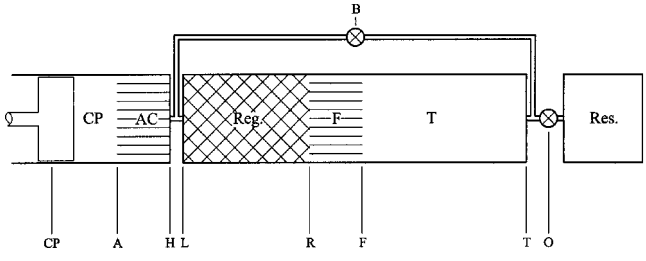

Fig. 1 Pulse-tube refrigerator, configuration and indices: from left to right, volumes are CP, compressor; AC, aftercooler; Reg, regenerator; F, freezer; T, pulse tube proper; and Res, reservoir. Interfaces denoted with indices as shown; resistances (usually valves) are main orifice O and bypass B.

Briefly, that this device produces refrigeration can be explained as follows. With its high thermal mass and good heat transfer capability, the regenerator works as a heat sponge, so that a nearly time-independent temperature gradient is maintained between its two extremities. As a result, in the first approximation, on both sides, the fluid returns from the regenerator at the same temperature as it entered, and there is little energy exchange between the two sides. There is, however, a large entropy exchange. Indeed, if there are no significant energy exchanges, then any work done by the compressor must leave the system in the aftercooler, carrying a substantial entropy flux out of the system ($\mathrm{d}S = \mathrm{d}Q/T$), which has nowhere to come from except the regenerator. On the other side of the regenerator, in the first approximation, isentropic flow occurs in the tube connecting the region at low temperature to the orifice, which is at ambient temperature and effectively also works as a heat exchanger. Thus, if the entropy delivered by the regenerator at its warm end is larger than the entropy sources due to internal losses, heat is absorbed in the freezer. In the absence of other losses besides the inherent irreversibility due to throttling in the orifice, this simple model yields a coefficient of performance (COP; the ratio refrigeration/compressor power), equal to the temperature ratio, as first noted by Kittel.[20]

It was shown in the preceding section that a nonzero leading-order pressure gradient results in a nonzero gradient in the leading-order entropy flux; thus, there is entropy created at leading order. The entropy sources due to thermal irreversibilities are of smaller order in M^2, however, and so is the enthalpy flux. As a result, to leading order, work and heat still balance each other at both ends of the regenerator even in the presence of a nonzero leading-order pressure gradient. The heat out at the aftercooler end of the pulse tube, hence also the compressor work, equals the entropy flux coming out of the regenerator at that end times the aftercooler temperature. Refrigeration equals the entropy flux into the regenerator at the freezer end times the freezer temperature. When these fluxes are equal, this results obviously in the Kittel COP.[20] Otherwise, that value is multiplied by the ratio of the entropy fluxes (from the freezer/into the aftercooler), which is less than unity.

The pressure gradients in the regenerator also affect performance in a different and more subtle way. The energy fluxes, and hence the refrigeration produced, are strongly dependent on the amplitude and phase relationship between pressure and velocity throughout the device. Quantification requires the whole design to be taken into account. However, the additional assumption that amplitudes are small is introduced, which turns out to be fairly accurate in typical pulse-tube devices. Indeed, the only way to reduce the impact of transition losses to an acceptable level is to limit amplitudes.[4,21] The low-amplitude approximation reduces the problem under consideration to a linear problem, potentially with closed-form solutions.

Small Amplitude

The small-amplitude model originates in the phasor diagrams introduced by Storch and Radebaugh.[6] The following model closely matches the approach by Bauwens.[4] All volumes are taken to be of the same order. The compressor displacement is small compared with the other volumes, in a ratio ϵ between volumetric compressor amplitude and net regenerator volume. When all volumes are scaled by the regenerator volume, the compressor motion is then given by

$$U_{\mathrm{CP}} = \epsilon(\exp 2\pi i t + \exp -2\pi i t) = 2\epsilon Re[\exp 2\pi i t] \tag{20}$$

Then velocities in all spaces including the regenerator (except the orifices) are of order ϵ. The solution is sinusoidal, $U = \epsilon u(X) \exp 2\pi i t$. When the mean pressure is used as the reference pressure, $P = 1 + \epsilon p(X) \exp 2\pi i t$. The regenerator model becomes

$$2\pi i \frac{p}{T} + \frac{\mathrm{d}}{\mathrm{d}X}\left(\frac{u}{T}\right) = 0 \tag{21a}$$

$$\frac{\mathrm{d}p}{\mathrm{d}X} = -fu \tag{21b}$$

$$T = T(X) \tag{21c}$$

The friction factor f approaches its constant laminar limit. In the small-amplitude limit, the entropy flux given by Eq. (19) becomes

$$\dot{S}(X) = \frac{(\gamma - 1)}{\gamma f T} \frac{\mathrm{d}(p^* p)}{\mathrm{d}X} \tag{22}$$

and, consequently, the COP is given by

$$\mathrm{COP} = \frac{\mathrm{d}(p^* p)/\mathrm{d}X|_{\mathrm{freezer}}}{\mathrm{d}(p^* p)/\mathrm{d}X|_{\mathrm{aftercooler}}} \tag{23}$$

Representation of the Various Volumes

The boundary conditions at the regenerator ends depend on the entire device configuration shown in Fig. 1. In the ducts, the pulse-tube proper, the reservoir, and the compressor, the flow is taken to be one-dimensional and isentropic but not necessarily homentropic. In particular in the tube, the transition from low to high temperature requires a nontrivial entropy stratification. Furthermore, the lengths are short compared to acoustic wavelengths, and viscous forces are small; pressure is approximately uniform, although time dependent. When density is eliminated between the mass and entropy equations, and it is taken into account that the period is unity and going to Fourier space, the relationship between pressure and velocity is[4]

$$\frac{1}{\gamma} 2i\pi p + \frac{\mathrm{d}u}{\mathrm{d}X} = 0 \tag{24}$$

In the heat exchangers, the flow is approximately isothermal. For constant temperature, in Fourier space, mass conservation yields

$$2i\pi p + \frac{\mathrm{d}u}{\mathrm{d}X} = 0 \tag{25}$$

These equations are readily integrated in space, reducing each volume into an impedance relating the difference in velocity at its ends with the time derivative of pressure. Furthermore, in the small-amplitude limit, the effect of transition losses[21] is relegated to smaller order in ϵ (Ref. 4); thus, density is continuous at the interfaces between spaces, hence so is the volumetric flow. If U is defined as the volumetric flow corresponding to a regenerator with unit cross section, then, after integration with respect to length, the change in volumetric flow is related to pressure by the following relationship for isentropic tubes:

$$V 2i\pi p + \gamma(u_{\mathrm{right}} - u_{\mathrm{left}}) = 0 \tag{26}$$

In spaces where temperature is constant, a similar relationship is obtained, replacing γ by 1.

The tube and reservoir are separated by an orifice, across which a significant pressure drop occurs; likewise, the bypass includes a valve, and these flow restrictions need a model. In a slender orifice, longitudinal diffusion is negligible, but transverse diffusion is not. If, furthermore, the length of the orifice is short compared to the sweep by the flow, then the flow becomes quasi steady, and all time derivatives are negligible. In particular, mass conservation then results in a spatially uniform mass flow rate ρu, and the inertia terms are negligible in the momentum equation. Finally, for velocities smaller than the speed of sound, acceleration terms are negligible. This yields the familiar Poiseuille parabolic velocity profile, which integrated over the cross-section and over the orifice length results in a simple resistive model:

$$[p] = -\gamma \Omega u \tag{27}$$

The mass flow rate is uniform along the orifice; thus, so is u. The resistance Ω obviously depends on the orifice properties.[4,22] The admittance $\mathcal{A} = 1/\Omega$ is useful because a fully closed orifice, a reachable and realistic limit, corresponds to a zero admittance.

Finally, at the extremities of the bypass, mass conservation yields a Kirchhoff law: The net sum of the mass flows coming from all branches is zero.

When these various components are taken into account, indices are used as shown on Fig. 1, and V is used for the various volumes, algebraic equations are obtained.

For the various spaces,

$$2\pi i p_R V_F + u_F - u_R = 0 \tag{28a}$$

$$2\pi i p_R V_T + \gamma(u_T - u_F) = 0 \tag{28b}$$

$$2\pi i p_R V_{\mathrm{res}} - \gamma u_O = 0 \tag{28c}$$

$$2\pi i p_L V_{\mathrm{AC}} + u_H - u_A = 0 \tag{28d}$$

$$2\pi i p_L V_{\mathrm{CP}} + \gamma(u_A - u_{\mathrm{CP}}) = 0 \tag{28e}$$

For the orifice resistances,

$$p_{\mathrm{res}} - p_R = -\gamma \Omega_O u_O \tag{29a}$$

$$p_R - p_L = -\gamma \Omega_B u_B \tag{29b}$$

For the bypass connections,

$$u_L + u_B = u_H \tag{30a}$$

$$u_O = u_T + u_B \tag{30b}$$

For the compressor amplitude, $u_{\mathrm{CP}} = 1$. After elimination, the following boundary conditions to the regenerator problem are obtained:

$$\gamma u_L = \gamma + (p_R - p_L)/\Omega_B - 2\pi i p_L V_L \tag{31a}$$

$$\gamma u_R = (p_R - p_L)/\Omega_B + 2\pi i p_R V_R \tag{31b}$$

in which V_R and V_L have been used:

$$V_L = \gamma V_{\mathrm{AC}} + V_{\mathrm{CP}} \tag{32a}$$

$$V_R = \frac{V_{\mathrm{res}}}{1 + 2\pi i \Omega_O V_{\mathrm{res}}} + \gamma V_F + V_T \tag{32b}$$

These boundary conditions correspond to a configuration including the bypass shown in Fig. 1. The case without bypass is readily dealt with setting $\Omega_B \to \infty$. The right boundary condition is homogeneous. Because of the forcing produced by the compressor, the left boundary condition is not homogeneous.

Exact Solutions

Problem Formulation

The problem consists of Eqs. (21) with boundary conditions, respectively, at $X = 0$ and 1, given by Eqs. (31), in which $T(X)$ is known. Eliminating velocity yields a second-order problem for $p(X)$ with mixed boundary conditions if the configuration includes a bypass. With $p_L = p(0)$ and $p_R = p(1)$,

$$T \frac{\mathrm{d}}{\mathrm{d}X}\left(\frac{1}{T}\frac{\mathrm{d}p}{\mathrm{d}X}\right) - 2f\pi i p = 0 \tag{33a}$$

$$\frac{\gamma}{f}\frac{\mathrm{d}p}{\mathrm{d}X}\bigg|_L + \gamma + \frac{p_R - p_L}{\Omega_B} - 2\pi i p_L V_L = 0 \tag{33b}$$

$$\frac{\gamma}{f}\frac{\mathrm{d}p}{\mathrm{d}X}\bigg|_R + \frac{p_R - p_L}{\Omega_B} + 2\pi i p_R V_R = 0 \tag{33c}$$

For the two specific temperature profiles shown in Fig. 2, exponential and linear, respectively, closed-form solutions exist. Although the actual profile will not be either of these, if both the linear and exponential profile yield results close to each other, then it is reasonable to infer that results for other similar profiles, including the correct one, will also be close. In the absence of specific information,

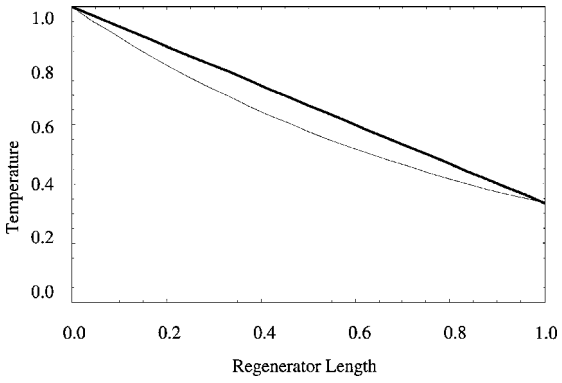

Fig. 2 Regenerator temperature profiles: thick line, linear profile and thin line, exponential profile. (Temperature and length are dimensionless.)

the linear profile has often been taken as an assumption by virtue of its apparent simplicity.[8,23]

Linear Profile

For the linear temperature profile,

$$\frac{1}{T}\frac{\mathrm{d}T}{\mathrm{d}X} = \frac{1}{X-c}, \qquad c = \frac{T(X_L)}{T(X_L)-T(X_R)} \tag{34}$$

so that Eq. (33a) becomes

$$(X-c)\frac{\mathrm{d}^2p}{\mathrm{d}X^2} - \frac{\mathrm{d}p}{\mathrm{d}X} - 2\pi if(X-c)p = 0 \tag{35}$$

the solution of which is

$$p = (X-c)\left\{C_1 J_1\left[i\sqrt{2\pi if}(X-c)\right] + C_2 Y_1\left[i\sqrt{2\pi if}(X-c)\right]\right\} \tag{36}$$

The boundary conditions determine the integration constants C_1 and C_2 (see Appendix A). Closed-form expressions for COP and refrigeration are obtained, respectively, from Eq. (23) and from knowing that refrigeration equals $-(\gamma-1)(up^* + u^*p)/\gamma$, evaluated in the freezer.

Exponential Profile

If the temperature profile is exponential, then the equation has constant coefficients and the solution is simpler. The profile is given by

$$\frac{1}{T}\frac{\mathrm{d}T}{\mathrm{d}X} = 2a, \qquad 2a = \log T(X_R) - \log T(X_L) \tag{37}$$

so that the differential equation becomes

$$\frac{\mathrm{d}^2p}{\mathrm{d}X^2} - 2a\frac{\mathrm{d}p}{\mathrm{d}X} - 2\pi ifp = 0 \tag{38}$$

The solution is

$$p = \exp aX\{C_1\exp[(m+in)X] + C_2\exp[-(m+in)X]\} \tag{39}$$

in which the constants m and n are defined as

$$m = \left(1/\sqrt{2}\right)\sqrt{\sqrt{a^4+4\pi^2f^2}+a^2} \tag{40a}$$

$$n = \left(1/\sqrt{2}\right)\sqrt{\sqrt{a^4+4\pi^2f^2}-a^2} \tag{40b}$$

and again, the integration constants C_1 and C_2 are readily determined by the boundary conditions (see Appendix B).

Results and Discussion

Configuration and Operating Conditions

Detailed solutions were obtained, for both the linear and exponential temperature profiles, for a pulse-tube cryocooler configured as follows. The temperature ratio was taken to be $\frac{1}{3}$. Expressed as fractions of the regenerator volume, the other volumes were $V_{\mathrm{res}} = 369$, $V_T = 1.00$, $V_{\mathrm{CP}} = 2.77$, $V_{\mathrm{AC}} = 1.55$, and $V_F = 0.94$. The values $\gamma = 1.6$ and $f = 0.05$ were used. The orifice resistances were varied over a range of values. These parameters were selected because they are in the same range as in a prototype developed in Calgary, which yields a no-load temperature of 50 K. All results shown are dimensionless. The dependency in both frequency and actual piston displacement are incorporated in the small parameter ϵ.

Pressure Amplitude and Phase in the Regenerator

For the specific value $\Omega_O = 0.1$ of the orifice resistance, the longitudinal profiles of pressure amplitude, that is the real part of the complex amplitude, and phase difference between pressure and velocity along the regenerator were obtained. They are shown in Fig. 3 for a configuration without a bypass and in Fig. 4 for a configuration with a bypass with resistance $\Omega_B = 0.05$, respectively. These results are shown for both the linear and exponential temperature profiles. In all cases, pressure lags behind the forcing oscillation. These results are consistent qualitatively and in magnitude with preliminary experimental results.

The bypass results in a significantly smaller drop in pressure amplitude and also in a reduction in the phase shift across the regenerator. The increased pressure amplitude at the cold end and the decrease in the phase angle both improve performance. Not only have the irreversibilities been reduced, but more important, the higher value of the product up^* shows an increase in refrigeration.

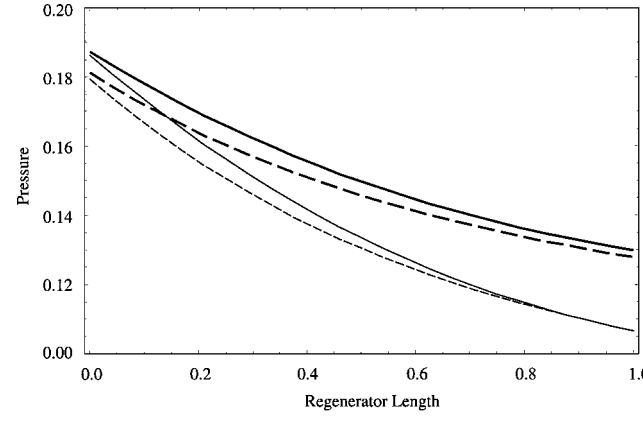

Fig. 3 Pressure amplitude along the regenerator length: orifice resistance Ω_O = 0.10: thick lines, bypass with resistance Ω_B = 0.05; thin lines, no bypass; continuous lines, linear temperature profile; and broken lines, exponential profile (pressure and length dimensionless).

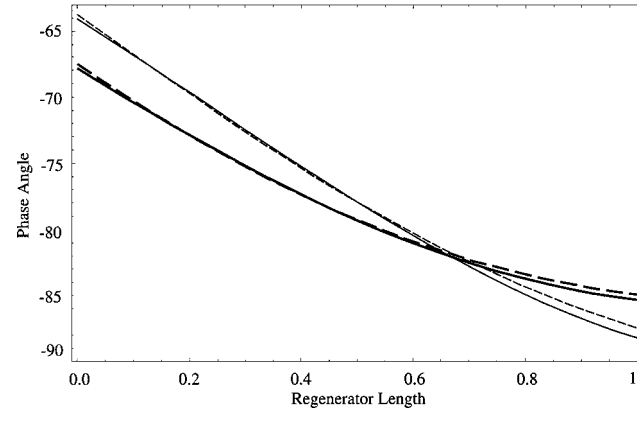

Fig. 4 Pressure phase angle along the regenerator length; same notation as Fig. 3.

In other words, the refrigerator is better designed overall, producing a higher output before losses. Because many losses, such as conduction or radiation losses, are more or less independent of the refrigeration produced, the net efficiency including the effect of all loss mechanisms not included in the current model should improve even more.

Differences are noticeable between the two temperature profiles in the amplitude results, whereas the difference in the phase shifts is insignificant. One side effect of the difference in the two temperature profiles is that the total mass of fluid in the regenerator is larger for the exponential profile, hence the somewhat decreased pressure amplitude at the warm end. This could be corrected by adjusting somewhat the piston amplitude to the specific profile instead of simply using the same value.

Effect of Orifice and Bypass Impedance on Performance

Introduction of the bypass increases the amplitude of the pressure fluctuation on the cold side and reduces the phase angle, with clear effects on performance. However, from experiments, the results are known to be quite sensitive to the bypass resistance, and the optimal bypass resistance is known to depend on the main orifice resistance. Likewise, even without taking the pressure gradient in the regenerator into account, it is clear that there is an optimal value of the orifice resistance.[4,5]

To study these issues, numerical results from both earlier solutions were obtained for a range of values of both resistances (or admittances). Figure 5 shows contour plots of the coefficient of performance for an array of values of both admittances, for both the linear and exponential temperature profile, whereas Fig. 6 shows the refrigeration. Figures 7 and 8 show the pressure drop across the regenerator and the phase at the cold end, respectively, for the linear temperature profile. (Results for the exponential profile are undistinguishable.)

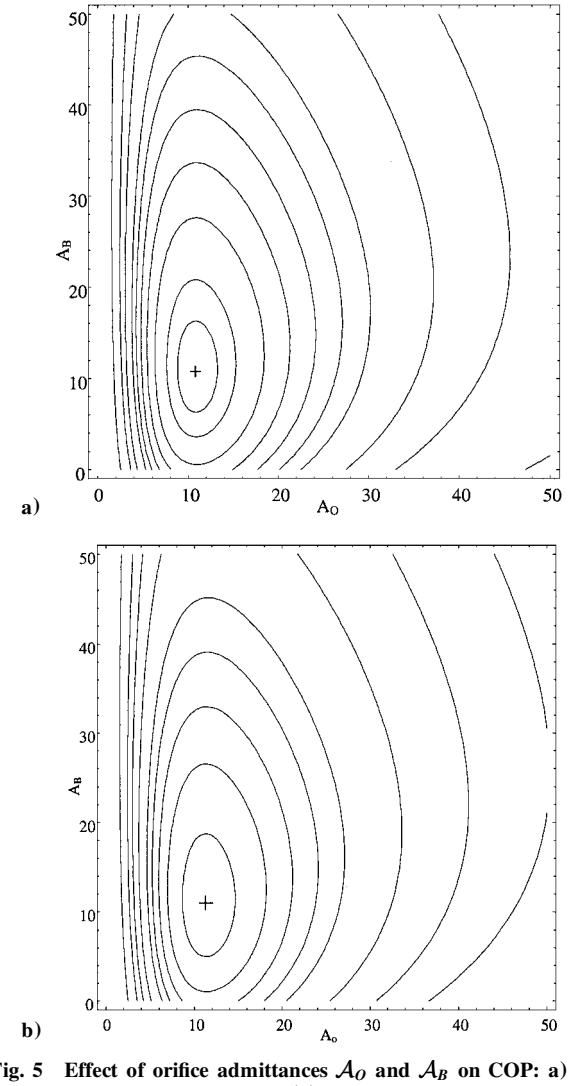

Fig. 5 Effect of orifice admittances $\mathcal{A}_O$ and $\mathcal{A}_B$ on COP: a) linear temperature profile, peak COP (+) = 0.149, from peak, level curves correspond to 0.1475, 0.1450, 0.140, 0.130, 0.125, 0.120, 0.110, 0.100, and 0.080; and b) exponential profile, peak COP = 0.152, level curves correspond to 0.150, 0.1450, 0.140, 0.130, 0.125, 0.120, 0.110, 0.100, and 0.080.

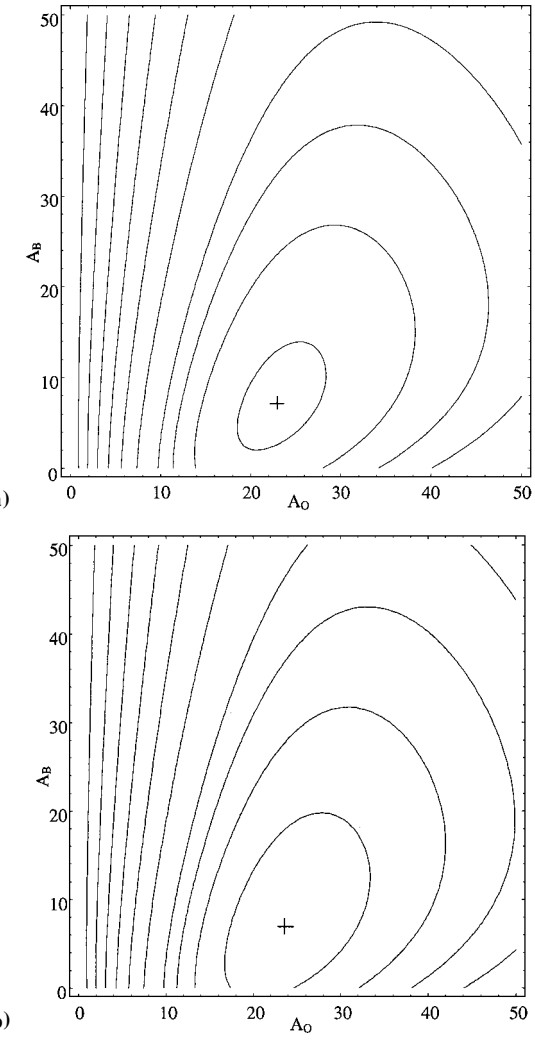

Fig. 6 Effect of orifice admittances $\mathcal{A}_O$ and $\mathcal{A}_B$ on refrigeration: a) linear temperature profile, peak refrigeration (+) = 0.043, from peak, level curves correspond to 0.0425, 0.0400, 0.0375, 0.0350, 0.030, 0.0250, 0.0200, 0.0150, 0.0100, and 0.0050; and b) exponential profile, peak = 0.044, level curves correspond to 0.0425, 0.0400, 0.0375, 0.0350, 0.030, 0.0250, 0.0200, 0.0150, 0.0100, and 0.0050.

First, these results show that there is a minimal difference between the two assumed temperature profiles, confirming that the impact of small variations in the profile is much below the effect of other uncertainties. Second, the COP and refrigeration results show a clear maximum for both, confirming that the interaction between pressure gradients in the regenerator and flow in the bypass plays at least some role. This is one explanation (although not necessarily the only one) for an observation by Zhu et al.[19] that adding a bypass may lead to a substantial performance improvement. The results are also at least qualitatively consistent with preliminary experimental results in the current prototype, which also show a much improved performance with a bypass, and clearly show that optimal values exist for both admittances. (Results are not expected to be quantitatively comparable with experiments because of all other sources of losses, many of which depend on a set of design parameters that are unrelated to the basic thermal/flow configuration.)

The maximum COP is reached roughly for the same bypass opening as for peak refrigeration, but with an orifice with approximately

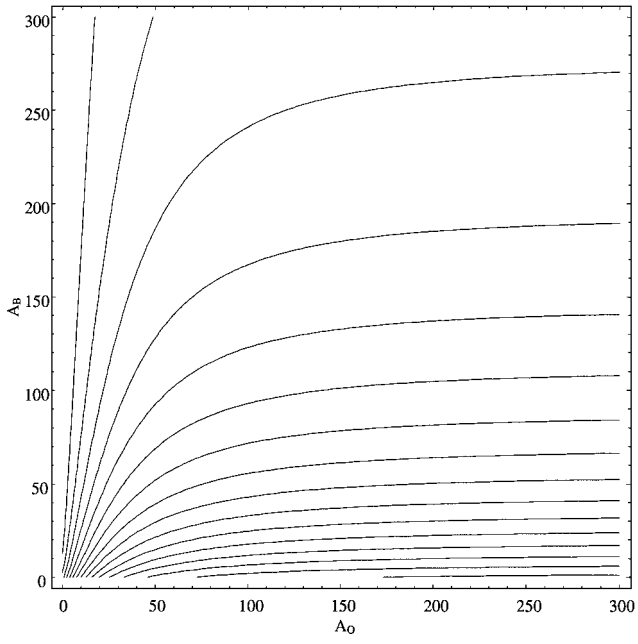

Fig. 7 Effect of orifice admittances $\mathcal{A}_O$ and $\mathcal{A}_B$ on regenerator pressure drop, linear temperature profile: from 0.16 (bottom), level curves correspond to sequence 0.01, 0.02, 0.03, 0.04, 0.05, 0.06, 0.07, 0.08, 0.09, 0.1, 0.11, 0.12, 0.13, 0.14, 0.15, and 0.16.

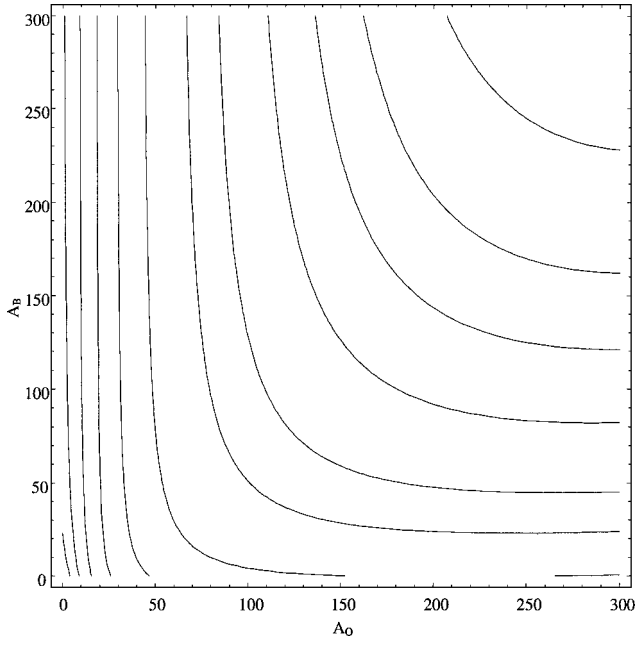

Fig. 8 Effect of orifice admittances $\mathcal{A}_O$ and $\mathcal{A}_B$ on pressure phase angle in freezer, linear temperature profile: from − 100 deg (bottom left) level curves correspond to sequence − 100, − 90, − 90, − 80, − 70, − 60, − 50, − 40, − 30, − 27, − 25, and − 23 deg.

double the resistance, hence less flow and a lower pressure gradient. That is probably a predictable result; however, one should expect that, when other losses are taken into account, the point of peak efficiency will shift closer to the point of peak refrigeration.

Performance Without a Bypass

Results for a configuration without a bypass correspond to the limit for zero bypass admittance, that is, the x axis on Figs. 5–8. However, these results are easier to read in Fig. 9, which shows refrigeration and COP vs the orifice admittance, for both linear and exponential temperature profiles. Again, the two temperature profiles yield results that are very close. Also, Fig. 9 clearly shows that

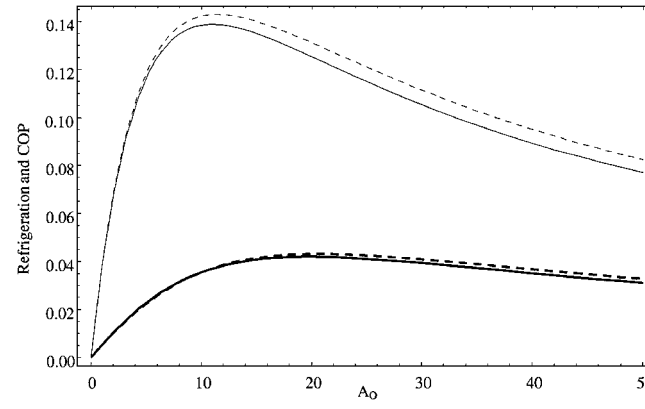

Fig. 9 Refrigeration and coefficient of performance vs orifice admittance $\mathcal{A}_O$, no bypass: thick lines, refrigeration; thin lines, COP; continuous lines, linear temperature profile; and broken lines, exponential profile.

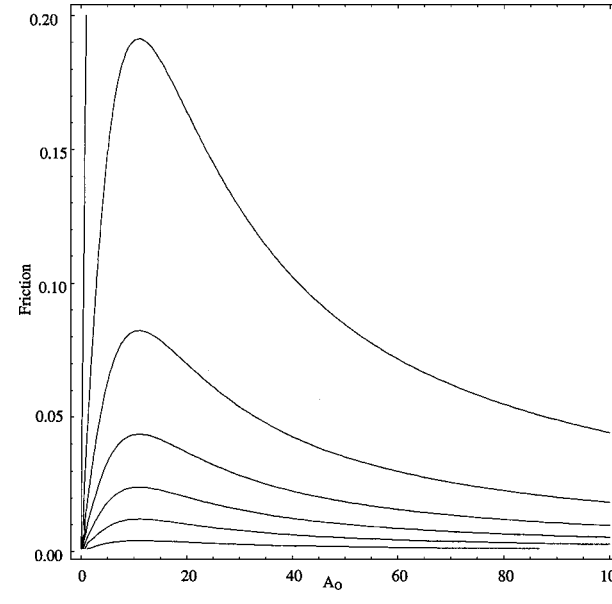

Fig. 10 Effect of orifice admittance $\mathcal{A}_O$ and friction factor f on coefficient of performance, no bypass, linear temperature profile: from 0.3 (bottom), level curves correspond to 0.01, 0.05, 0.1, 0.15, 0.2, 0.25, and 0.3.

optimal orifice admittance values exist that maximize refrigeration or COP.

The key parameter characterizing the regenerator matrix is the friction factor f. Figures 10 and 11 present contour plots of the COP and refrigeration for an array of values of the friction factor and the orifice admittance. (Only results for the linear temperature profile are shown; the exponential profile yields very similar values.) As expected, both COP and refrigeration decrease with friction because 1) friction is irreversible and 2) the product up^* in the freezer decreases as the pressure drop across the regenerator goes up. The COP approaches 0.33 as friction approaches zero, which is indeed the ideal Kittel COP[20] at the temperature ratio of $\frac{1}{3}$.

The maximum refrigeration point continues existing in the limit of zero friction. However, as friction approaches zero, in contrast to the COP that approaches the ideal limit for all values of the orifice admittance, refrigeration remains strongly dependent on the orifice admittance. Indeed, refrigeration is proportional to the product up^* in the freezer, whereas the COP, as shown in Eq. (23), is given by the ratio of the products up^* at the warm end of regenerator and in the freezer, as discussed earlier. Likewise, the peak COP and the peak refrigeration move away from each other as friction increases.

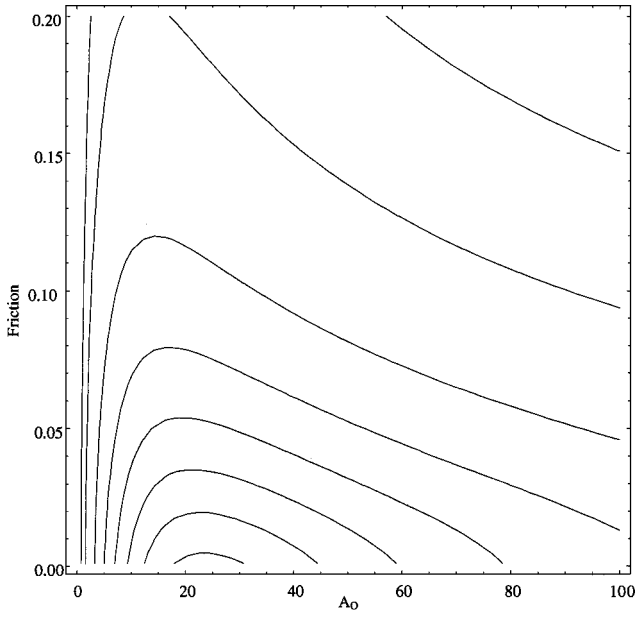

Fig. 11 Effect of orifice admittance $\mathcal{A}_O$ and friction factor f on refrigeration, no bypass, linear temperature profile: from 0.070 (bottom), level curves correspond to 0.005, 0.010, 0.020, 0.030, 0.040, 0.050, 0.060, and 0.070.

Conclusions

This study included two main parts. First, an asymptotically consistent simplified regenerator model was developed. It includes exact one-dimensional continuity. In the momentum equation, inertia effects can be neglected, the leading-order pressure gradient is related through a Darcy law to the local cross-section-averaged instantaneous velocity, and the friction factor depends on the local and instantaneous Reynolds number. Finally, because flow passages are small and the matrix has high thermal mass, temperatures are time independent, but obviously not uniform lengthwise.

In the second part, this model was applied to a complete pulse-tube cryocooler with a complex configuration, including a bypass and, hence, two parallel flow paths. An additional approximation was also made, that amplitudes are small, in which case the nonlinear effect of the gas law on compressibility becomes negligible. That assumption, which is often made in studies of pulse-tube refrigerators,[4,6,22] is usually reasonably accurate for these devices; it leads to a harmonic behavior in time and a linear model in space, which lends itself to a closed-form solution.

The physical model includes the piston motion, the volume distribution, the bypass, the orifice, and the idealized representation of the flow in the regenerator. The results reveal a complex behavior, in particular with respect to the effect of orifice and bypass adjustment. That is not overly surprising because instantaneous division of the flow between the two parallel paths depends on the instantaneous impedances of the two paths. Although simplified in relation to the full set of compressible Navier–Stokes equations, the model that was used to predict the relationship between flow and pressure drop in the regenerator is still a fairly sophisticated one, especially considering that it was coupled with the complex geometrical description.

The results show that, in the presence of relatively high pressure gradients in the regenerator, the bypass improves performance by reducing these gradients and by improving the phase relationship between pressure and velocity in the freezer.

The only assumption that was not based on a proper limit process refers to the regenerator temperature profile. However, the results show that within a reasonable range, which will normally include the exact profile, the uncertainty due to small inaccuracies in the temperatures is small, particularly in comparison with uncertainties due to the limitations of the physical model. The model is fundamental, and except for the temperature profile assumption and the numerical value of the friction factor, it stands on its own without the need for experimental validation. The friction factor depends on instantaneous Reynolds number and matrix topology; experimental determination is required.

Because it leads to a mathematical problem that is solved in closed-form and, hence, there is no need for iterations and no discretization errors, the current performance prediction tool yields results quickly, accurately, and effectively.

Appendix A: Integration Constants (Linear Temperature Profile)

The values of the integration constants C_1 and C_2 appearing in Eq. (36) are determined expressing that the solution satisfies the boundary conditions, Eqs. (31):

$$C_1 = \frac{-\gamma N_4}{N_1 N_4 - N_2 N_3}, \qquad C_2 = \frac{-\gamma N_2}{N_1 N_4 - N_2 N_3}$$

in which, for the pulse tube with a bypass, the constants N_i are

$$N_1 = \frac{(1-c)J_1[ib(1-c)]}{\Omega_B} + c\left(2i\pi V_L + \frac{1}{\Omega_B}\right)J_1(-ibc) + \frac{\gamma\left\{J_1(-ibc) - \frac{1}{2}ibc[J_0(-ibc) - J_2(-ibc)]\right\}}{f}$$

$$N_2 = (c-1)\left(2i\pi V_R + \frac{1}{\Omega_B}\right)J_1[ib(1-c)] + \frac{cJ_1(-ibc)}{\Omega_B} - \frac{\gamma\left(J_1[ib(1-c)] + \frac{1}{2}ib(1-c)\{J_0[ib(1-c)] - J_2[ib(1-c)]\}\right)}{f}$$

$$N_3 = \frac{(1-c)Y_1[ib(1-c)]}{\Omega_B} + c\left(2i\pi V_L + \frac{1}{\Omega_B}\right)Y_1(-ibc) + \frac{\gamma\left\{Y_1(-ibc) - \frac{1}{2}ibc[Y_0(-ibc) - Y_2(-ibc)]\right\}}{f}$$

$$N_4 = (1-c)\left(2i\pi V_R + \frac{1}{\Omega_B}\right)Y_1[ib(1-c)] + \frac{cY_1(-ibc)}{\Omega_B} + \frac{\gamma\left(Y_1[ib(1-c)] + \frac{1}{2}ib(1-c)\{Y_0[ib(1-c)] - Y_2[ib(1-c)]\}\right)}{f}$$

If there is no bypass, then by setting $\Omega_B \to \infty$, the solution simplifies,

$$N_1 = 2c\pi V_L J_1(-bc) + \frac{\gamma\left\{J_1(-bc) - \frac{1}{2}bc[J_0(-bc) - J_2(-bc)]\right\}}{f}$$

$$N_2 = 2(c-1)\pi V_R J_1[b(1-c)] - \frac{\gamma\left(J_1[b(1-c)] + \frac{1}{2}b(1-c)\{J_0[b(1-c)] - J_2[b(1-c)]\}\right)}{f}$$

$$N_3 = 2c\pi V_L Y_1(-bc) + \frac{\gamma\left\{Y_1(-bc) - \frac{1}{2}bc[Y_0(-bc) - Y_2(-bc)]\right\}}{f}$$

$$N_4 = 2(1-c)\pi V_R Y_1[b(1-c)] + \frac{\gamma\left(Y_1[b(1-c)] + \frac{1}{2}b(1-c)\{Y_0[b(1-c)] - Y_2[b(1-c)]\}\right)}{f}$$

where

$$b = \sqrt{2\pi f i}$$

Appendix B: Integration Constants (Exponential Temperature Profile)

Again, the integration constants C_1 and C_2 appearing in Eq. (38) are determined from the boundary conditions, Eqs. (31). With a bypass,

$$C_1 = \frac{\exp(Z) f \{\exp(a+Z)[(a+Z)\gamma + 2\pi f i V_R] + f[1+\exp(a+Z)]/\Omega_B\}}{N_1}$$

$$C_2 = -\frac{\exp(-Z)\{\exp(a)[(Z-a)\gamma - 2\pi f i V_R] - f[\exp(a)+\exp(Z)]/\Omega_B\}}{f N_2}$$

where

$$N_1 = \exp(a)\big(4\pi^2 f^2[\exp(2Z)-1]V_L V_R + [\exp(2Z)-1] \times (Z^2-a^2)\gamma^2 - 2\pi f \gamma i\{a[\exp(2Z)-1](V_L+V_R) + Z[1+\exp(2Z)](V_L-V_R)\}\big) + 2f\{\gamma Z[\exp(Z) - \exp(2a+Z)] + \exp(a)[if\pi(V_L+V_R) + a\gamma] - i\exp(a+2Z)[\pi f(V_L+V_R) - ia\gamma]\}/\Omega_B$$

$$N_2 = \{[\gamma(a+Z)/f + 2i\pi V_R + 1/\Omega_B]\exp(a+Z) + 1/\Omega_B\} \times [2i\pi V_L + (a-Z)\gamma/f + 1 + \exp(a-Z)/\Omega_B] - \{[\gamma(a-Z)/f + 2i\pi V_R + 1/\Omega_B]\exp(a-Z) + 1/\Omega_B\} \times [2i\pi V_L + (a+Z)\gamma/f + 1 + \exp(a+Z)/\Omega_B]$$

In the absence of a bypass, this simplifies to

$$C_1 = \frac{\exp(2Z) f [2\pi f i V_R + \gamma(a+Z)]}{N_1}$$

$$C_2 = -\frac{\exp(a-Z)[\gamma(Z-a) - 2\pi f i V_R]}{f N_2}$$

where

$$N_1 = 4\pi^2 f^2[\exp(2Z)-1]V_L V_R + \gamma^2[\exp(2Z)-1](Z^2-a^2) - 2\pi f \gamma i\{a[\exp(2Z)-1](V_L+V_R) + Z[1+\exp(2Z)](V_L-V_R)\}$$

$$N_2 = [2\pi V_L i + (a-Z)\gamma/f][2\pi V_R i \exp(a+Z) + \gamma(a+Z)\exp(a+Z)/f] - [2\pi V_R i \exp(a-Z) + \gamma(a-Z)\exp(a-Z)/f][2\pi V_L i + (a+Z)\gamma/f]$$

$$Z = \sqrt{a^2 + 2\pi f i}$$

Acknowledgment

This work was supported by the Natural Science and Engineering Research Council of Canada under the Strategic Projects program.

References

[1]Gifford, W., and Longsworth, R., "Pulse Tube Refrigeration," *Journal of Engineering for Industry, Series B*, Vol. 86, No. 3, 1964, pp. 264–268.

[2]Radebaugh, R., "A Review of Pulse Tube Refrigeration," *Advances in Cryogenic Engineering*, Vol. 35B, 1990, pp. 1191–1206.

[3]Mikulin, E. I., Tarasov, A. A., and Shkrebyonock, M. P., "Low Temperature Expansion Pulse Tube," *Advances in Cryogenic Engineering*, Vol. 29, 1984, pp. 629–638.

[4]Bauwens, L., "Interface Loss in the Small Amplitude Orifice Pulse-Tube Model," *Advances in Cryogenic Engineering*, Vol. 43B, 1998, pp. 1933–1940.

[5]Mirels, H., "Linearized Theory for Pulse Tube Cryocooler Performance," *AIAA Journal*, Vol. 32, No. 8, 1994, pp. 1662–1669.

[6]Storch, P. J., and Radebaugh, R., "Development and Experimental Test of an Analytical Model of the Orifice Pulse Tube Refrigerator," *Advances in Cryogenic Engineering*, Vol. 33, 1988, pp. 851–859.

[7]Bauwens, L., "Oscillating Flow of a Heat-Conducting Fluid in a Narrow Tube," *Journal of Fluid Mechanics*, Vol. 324, 1996, pp. 135–161.

[8]Urieli, I., and Berchowitz, D. M., *Stirling Cycle Engine Analysis*, Adam Hilger, Bristol, England, U.K., 1984, pp. 21, 88.

[9]Deng, X., Mayzus, P., Fang, L., Fauvel, O. R., and Bauwens, L., "Numerical Simulation of Pulse Tube Cryocoolers," *CHT'01: Advances in Computational Heat Transfer*, edited by G. de Vahl Davis and E. Leonardi, Begell House, New York, 2001, pp. 293–300.

[10]Gedeon, D., "Sage: Object-Oriented Software for Cryocooler Design," *Cryocoolers 8*, Plenum, New York, 1995, pp. 281–292.

[11]Graetz, L., "Über die Wärmeleitfähigkeit von Flüßingkeiten," *Annals of Physics*, Vol. 25, 1885, pp. 337–342.

[12]Bauwens, L., Deng, X., Fang, L., and P. Mayzus, P., "Oscillating Flows in Porous Media and Proper Formulations for Regenerator Analysis," *Proceedings of the 10th International Stirling Engine Conference*, VDI-Gesellschaft, Dusseldorf, Germany, 2002, pp. 25–32.

[13]Bear, J., *Dynamics of Fluids in Porous Media*, American Elsevier, New York, 1972.

[14]Bauwens, L., "Entropy Balance and Performance Characterization of the Narrow Basic Pulse-Tube Refrigerator," *Journal of Thermophysics and Heat Transfer*, Vol. 10, No. 4, 1996, pp. 663–671.

[15]Xiao, J. H., "Thermoacoustic Theory for Cyclic Flow Regenerators," *Cryogenics*, Vol. 32, No. 10, 1992, pp. 895–901.

[16]Miyabe, H., Takahashi, S., and Hamaguchi, K., "An Approach to the Design of Stirling Engine Regenerator Matrix Using Packs of Wire Gauze," *Proceedings of the 17th Intersociety Energy Conversion Engineering Conference*, Inst. of Electrical and Electronics Engineers, Piscataway, NJ, 1982, pp. 1839–1848.

[17]Bauwens, L., "Near-Isothermal Regenerator: A Perturbation Analysis," *Journal of Thermophysics and Heat Transfer*, Vol. 9, No. 4, 1995, pp. 749–756.

[18]Bauwens, L., "Near-Isothermal Regenerator: Complete Thermal Characterization," *Journal of Thermophysics and Heat Transfer*, Vol. 12, No. 3, 1998, pp. 414–422.

[19]Zhu, S., Wu, P., and Chen, Z., "Double Inlet Pulse Tube Refrigerator: An Important Improvement," *Cryogenics*, Vol. 30, No. 6, 1990, pp. 514–520.

[20]Kittel, P., "Ideal Orifice Pulse Tube Refrigerator Performance," *Cryogenics*, Vol. 32, No. 9, 1992, pp. 843, 844.

[21]Kittel, P., "Enthalpy Flow Transition Losses in Regenerative Cryocoolers," U.S. Air Force Phillips Lab., Rept. PL-CP-93-1001, Kirtland, NM, 1993.

[22]Mirels, H., "Effect of Orifice Flow and Heat Transfer on Gas Spring Hysteresis," *AIAA Journal*, Vol. 32, No. 8, 1994, pp. 1656–1661.

[23]Qvale, E. B., and Smith, J. L., Jr., "An Approximate Solution for the Thermal Performance of a Stirling-Engine Regenerator," *Journal of Engineering for Power, Series A*, Vol. 91, No. 2, 1969, pp. 109–112.

J. P. Gore
Associate Editor